

OPEN ACCESS

The M3D- C^1 approach to simulating 3D 2-fluid magnetohydrodynamics in magnetic fusion experiments

To cite this article: S C Jardin *et al* 2008 *J. Phys.: Conf. Ser.* **125** 012044

View the [article online](#) for updates and enhancements.

You may also like

- [IPMC mechano-electrical transduction: its scalability and optimization](#)
D Pugal, P Solin, A Aabloo et al.
- [Modeling heat dominated electric breakdown in air, with adaptivity to electron or ion time scales](#)
A Agnihotri, W Hundsdoerfer and U Ebert
- [Blind backscattering experimental data collected in the field and an approximately globally convergent inverse algorithm](#)
Andrey V Kuzhuget, (UNCC/ChalmersGU team), Larisa Beilina et al.



Breath Biopsy[®] OMNI[®]

The most advanced, complete solution for global breath biomarker analysis

TRANSFORM YOUR RESEARCH WORKFLOW



Expert Study Design & Management



Robust Breath Collection



Reliable Sample Processing & Analysis



In-depth Data Analysis



Specialist Data Interpretation

The M3D- C^l approach to simulating 3D 2-fluid magnetohydrodynamics in magnetic fusion experiments

S. C. Jardin^{§1}, N. Ferraro¹, X. Luo², J. Chen¹, J. Breslau¹, K. E. Jansen², and M. S. Shephard²

¹Princeton Plasma Physics Laboratory, P.O. Box 451, Princeton NJ 08543

²Rensselaer Polytech Inst, Sci Computat Res Ctr, Troy, NY 12180

Abstract. A new approach for solving the 3D MHD equations in a strongly magnetized toroidal plasma is presented which uses high-order 2D finite elements with C^l continuity. The vector fields use a physics-based decomposition. An efficient implicit time advance separates the velocity and field advance. ITAPS (SCOREC) adaptivity software and TOPS solvers are used.

1. Introduction

The two-fluid MHD equations for a magnetized fusion-grade plasma are a high-order system of 8 scalar variables that are characterized by a wide range of space and timescales and by extreme anisotropy. The M3D code [1] has proven itself to be an invaluable tool for the simulation and understanding of global nonlinear phenomena in magnetic fusion confinement devices. However, the structure of M3D is not optimal for computing in regimes where two-fluid (2F) effects dominate, or for times that are very long compared to the Alfvén transit time. We have built upon many of the favorable features of the M3D approach to construct the M3D- C^l code [2], which is based on high-order, compact finite elements with C^l continuity on an unstructured adaptive triangle-based grid. The efficient split-implicit time advance is closely related to the ideal MHD energy principle, and allows time steps several orders of magnitude in excess of the Courant condition based on the Alfvén or whistler waves. Previous papers have described this technique applied to the 2F equations in 2D slab geometry. [2,3] In this paper, we discuss a subset of the full method as it is applied to the linearized single fluid MHD equations in 3D toroidal geometry.

2. Numerical method and definitions

We restrict consideration here to solutions linearized about an initial equilibrium with zero velocity, $\mathbf{V}_0 = 0$. The full 2F nonlinear solution, to be presented elsewhere, builds on the method presented here. The split linearized time advance [4,5] can be written as follows. First, introducing the implicit parameter ($0 < \theta < 1$), the velocity is advanced to the new time level (n+1) using the magnetic field at the half-time level (n+1/2):

$$\{\rho - \theta^2 (\delta t)^2 L\} \mathbf{V}^{n+1} = \{\rho - \theta^2 (\delta t)^2 L\} \mathbf{V}^n + \delta t \left\{ -\nabla p + \frac{1}{\mu_0} (\nabla \times \mathbf{B}) \times \mathbf{B} \right\}^{n+1/2} \quad (1)$$

Here ρ is the plasma density, p is the pressure, and L is the linear ideal MHD operator [6]:

$$L\{\mathbf{V}\} = \frac{1}{\mu_0} \left\{ \nabla \times [\nabla \times (\mathbf{V} \times \mathbf{B})] \right\} \times \mathbf{B} + \frac{1}{\mu_0} (\nabla \times \mathbf{B}) \times [\nabla \times (\mathbf{V} \times \mathbf{B})] + \nabla (\mathbf{V} \cdot \nabla p + \gamma p \nabla \cdot \mathbf{V}) \quad (2)$$

Next, the pressures, density, and magnetic field are advanced from time level (n+1/2) to (n+3/2) using the velocity at time (n+1). Defining $\theta_m \equiv 1 - \theta$, we have:

$$p^{n+3/2} = p^{n+1/2} - \delta t \left[\mathbf{V}^{n+1} \cdot (\theta \nabla p^{n+3/2} + \theta_m \nabla p^{n+1/2}) - \gamma (\theta p^{n+3/2} + \theta_m p^{n+1/2}) \nabla \cdot \mathbf{V}^{n+1} + S^{n+1/2} \right] \quad (3)$$

$$\mathbf{B}^{n+3/2} = \mathbf{B}^{n+1/2} + \delta t \nabla \times \left[\mathbf{V}^{n+1} \times (\theta \mathbf{B}^{n+3/2} + \theta_m \mathbf{B}^{n+1/2}) - \eta (\theta \nabla \times \mathbf{B}^{n+3/2} + \theta_m \nabla \times \mathbf{B}^{n+1/2}) \right] \quad (4)$$

[§] Corresponding author jardin@pppl.gov

This is unconditionally stable for all δt for implicit parameter $\theta \geq 1/2$. We use a physics-motivated decomposition of the vector fields in toroidal geometry. Using a cylindrical coordinate system (R, φ, Z) with $|\nabla \varphi| = 1/R$, we define the 2D gradient and 2D divergence operators as $\nabla_{\perp} a \equiv a_R \hat{R} + a_Z \hat{Z}$, $\nabla_{\perp} \cdot \mathbf{A} \equiv R^{-1} (R \mathbf{A} \cdot \hat{R})_R + (\mathbf{A} \cdot \hat{Z})_Z$. Subscripts denote partial differentiation with respect to R and Z . The velocity field is represented in terms of the three scalar variables (U, ω, χ) as follows: $\mathbf{V} = R^2 \nabla U \times \nabla \varphi + \omega R^2 \nabla \varphi + R^{-2} \nabla_{\perp} \chi$. The magnetic vector potential is given in terms of the two scalar variables (f, ψ) and the constant F_0 (proportional to the current in the toroidal field magnets) as: $\mathbf{A} = R^2 \nabla \varphi \times \nabla f + \psi \nabla \varphi - F_0 \ln R \hat{Z}$. Note that the gauge condition implied by this form is: $R^2 \nabla_{\perp} \cdot R^{-2} \mathbf{A} = 0$. The magnetic field and current density are calculated in terms of the vector potential variables as: $\mathbf{B} = \nabla \times \mathbf{A} = \nabla \psi \times \nabla \varphi - \nabla_{\perp} f' + F \nabla \varphi$ and $\mathbf{J} \equiv \nabla \times \mathbf{B} = \nabla F^* \times \nabla \varphi + R^{-2} \nabla_{\perp} \psi' - \Delta^* \psi \nabla \varphi$. Here we have defined auxiliary variables $F \equiv F_0 + R^2 \nabla \cdot \nabla_{\perp} f$, $F^* \equiv F_0 + R^2 \nabla^2 f = F + f''$, and the operator: $\Delta^* \psi \equiv R^2 \nabla_{\perp} \cdot R^{-2} \nabla \psi$. Primes denote differentiation with respect to the angle φ . Note that \mathbf{B} and \mathbf{J} are manifestly divergence free.

3. The scalar equations

Each of the scalar fields is divided into a 2D equilibrium part and a 3D perturbed part. Thus, for example: $\psi(R, \varphi, Z, t) = \psi_0(R, Z) + \psi_1(R, \varphi, Z, t)$. In the work described here, the velocity variables do not have an equilibrium part. All the equilibrium and perturbed variables are expanded in 2D basis functions for the Q_{18} triangular finite element with C^1 continuity [7], which we denote $v_i(R, Z)$. To get scalar forms for the momentum equation, we take the weak form of the three following projections of (1) and perform integration by parts as indicated in (5):

$$\begin{aligned} & \iint d^2 R v_i \nabla \varphi \cdot \nabla_{\perp} \times R^2 (1) & \iint d^2 R R^2 \nabla_{\perp} v_i \times \nabla \varphi \cdot (1) \\ & \iint d^2 R v_i R^2 \nabla \varphi \cdot (1) & \rightarrow & \iint d^2 R v_i R^2 \nabla \varphi \cdot (1) \\ & - \iint d^2 R v_i \nabla_{\perp} \cdot R^{-2} (1) & \iint d^2 R R^{-2} \nabla_{\perp} v_i \cdot (1) \end{aligned} \quad (5)$$

These projections, combined with the form of the velocity field described above, lead to energy conserving subsets of the full equations [8,9], and a partial decoupling of the part of the velocity field that does not compress the strong toroidal field. [10] The resulting scalar integrands can be written compactly in terms of the inner and Poisson brackets. For any two scalar variables a and b , we define: $(a, b) \equiv \nabla_{\perp} a \cdot \nabla_{\perp} b = a_R b_R + a_Z b_Z$ and $[a, b] \equiv [\nabla a \times \nabla b \cdot \nabla \varphi] = R^{-1} (a_Z b_R - a_R b_Z)$. The partial perturbed energies $\delta W_{ij}(a, b)$ [6] are defined in the Appendix. Thus, for (1) we have:

$$\begin{aligned} & \left\{ \rho R^2 (v_i, U^{n+1}) - \rho [v_i, \chi^{n+1}] - (\theta \delta t)^2 [\delta W_{11}(v_i, U^{n+1}) + \delta W_{12}(v_i, \omega^{n+1}) + \delta W_{13}(v_i, \chi^{n+1})] \right\} \\ & = \left\{ \rho R^2 (v_i, U^n) - \rho [v_i, \chi^n] - (\theta \delta t)^2 [\delta W_{11}(v_i, U^n) + \delta W_{12}(v_i, \omega^n) + \delta W_{13}(v_i, \chi^n)] \right\} \\ & + \delta t \left\{ \Delta^* \psi ([v_i, \psi] - (v_i, f')) + \frac{F}{R^2} (v_i, \psi') + F [v_i, f''] - R^2 [p, v_i] \right\}^n \end{aligned} \quad (6a)$$

$$\begin{aligned} & \left\{ \rho R^2 v_i \omega^{n+1} - (\theta \delta t)^2 \left[\delta W_{21}(v_i, U^{n+1}) + \delta W_{22}(v_i, \omega^{n+1}) + \delta W_{23}(v_i, \chi^{n+1}) \right] \right\} \\ & = \left\{ \rho R^2 v_i \omega^n - (\theta \delta t)^2 \left[\delta W_{21}(v_i, U^n) + \delta W_{22}(v_i, \omega^n) + \delta W_{23}(v_i, \chi^n) \right] \right\} \end{aligned} \quad (6b)$$

$$\begin{aligned} & + \delta t \left\{ -\frac{v_i}{R^2} (\psi, \psi') + v_i [f'', \psi] + v_i [F, \psi] + v_i [f', \psi'] - v_i (f', f'') - v_i (f', F) - v_i p' \right\}^n \\ & - \frac{\rho}{R^4} (v_i, \chi^{n+1}) - \rho [v_i, U^{n+1}] - (\theta \delta t)^2 \left[\delta W_{31}(v_i, U^{n+1}) + \delta W_{32}(v_i, \omega^{n+1}) + \delta W_{33}(v_i, \chi^{n+1}) \right] \\ & = -\frac{\rho}{R^2} (v_i, \chi^n) - \rho R^2 [v_i, U^n] - (\theta \delta t)^2 \left[\delta W_{31}(v_i, U^n) + \delta W_{32}(v_i, \omega^n) + \delta W_{33}(v_i, \chi^n) \right] \end{aligned} \quad (6c)$$

$$+ \delta t \left\{ \Delta^* \psi \frac{1}{R^2} \left[\frac{1}{R^2} (\psi, v_i) + [v_i, f'] \right] + \frac{F}{R^4} [(v_i, F) + (v_i, f'') - [v_i, \psi']] + \frac{1}{R^2} (v_i, p) \right\}^n$$

Similarly, taking appropriate projections of (4) gives the time advance integrands for the magnetic field variables:

$$\begin{aligned} & -\frac{1}{R^2} (v_i, \psi^{n+3/2}) - \theta \delta t \left\{ \frac{1}{R^2} (v_i, R^2 [\psi^{n+3/2}, U^{n+1}]) - \frac{F^{n+3/2}}{R^2} (v_i, U^{n+1}) + \frac{\omega^{n+1}}{R^2} (v_i, \psi^{n+3/2}) \right. \\ & \left. + \frac{1}{R^2} \left(v_i, \frac{1}{R^2} (\psi^{n+3/2}, \chi^{n+1}) \right) + \frac{1}{R^4} F^{n+3/2} [v_i, \chi^{n+1}] \right. \\ & \left. + \frac{\eta}{R^2} \left[\Delta^* v_i \Delta^* \psi^{n+3/2} - \frac{1}{R^2} (v_i, \psi^{n+3/2}) - [v_i, f^{n+3/2}] - [v_i, F^{n+3/2}] \right] \right\} \\ & = -\frac{1}{R^2} (v_i, \psi^{n+1/2}) + \theta_m \delta t \left\{ \frac{1}{R^2} (v_i, R^2 [\psi^{n+1/2}, U^{n+1}]) - \frac{F^{n+1/2}}{R^2} (v_i, U^{n+1}) + \frac{\omega^{n+1}}{R^2} (v_i, \psi^{n+1/2}) \right. \\ & \left. + \frac{1}{R^2} \left(v_i, \frac{1}{R^2} (\psi^{n+1/2}, \chi^{n+1}) \right) + \frac{1}{R^4} F^{n+1/2} [v_i, \chi^{n+1}] \right. \\ & \left. + \frac{\eta}{R^2} \left[\Delta^* v_i \Delta^* \psi^{n+1/2} - \frac{1}{R^2} (v_i, \psi^{n+1/2}) - [v_i, f^{n+1/2}] - [v_i, F^{n+1/2}] \right] \right\} \end{aligned} \quad (7a)$$

$$\begin{aligned} & \frac{v_i}{R^2} F^{n+3/2} - \theta \delta t \left\{ F^{n+3/2} [v_i, U^{n+1}] + \frac{1}{R^4} F^{n+3/2} (v_i, \chi^{n+1}) - \omega^{n+1} [v_i, \psi^{n+3/2}] \right. \\ & \left. - \frac{\eta}{R^2} (v_i, F^{n+3/2}) + -\frac{\eta}{R^2} (v_i, f^{n+3/2}) + \frac{\eta}{R^2} [v_i, \psi^{n+3/2}] \right\} \\ & = \frac{v_i}{R^2} F^{n+1/2} + \theta_m \delta t \left\{ F^{n+1/2} [v_i, U^{n+1}] + \frac{1}{R^4} F^{n+1/2} (v_i, \chi^{n+1}) - \omega^{n+1} [v_i, \psi^{n+1/2}] \right. \\ & \left. - \frac{\eta}{R^2} (v_i, F^{n+1/2}) + -\frac{\eta}{R^2} (v_i, f^{n+1/2}) + \frac{\eta}{R^2} [v_i, \psi^{n+1/2}] \right\} \end{aligned} \quad (7b)$$

4. Linearization and solution:

In the benchmarking results presented here, we eliminated the φ dependence by taking all the linearized variables to be complex and varying as $\exp[i n \varphi]$, where n is the toroidal mode number. This allows comparison with ideal MHD stability codes such as PEST [11] in the appropriate limit. We form a single matrix to solve for the velocity variables (6abc), and then subsequently form another to solve for the magnetic variables (7ab). For the linearized solution, we use SuperLU_dist [12] to factor the matrices into LU and then perform the backsolves each timestep.

5. Interfaces to support unstructured mesh

ITAPS and SCOREC have coordinated with CEMM and PPPL to support the use of ITAPS mesh adaptivity technologies in M3D-C^l. Four components have been added for applying parallel scalable adaptive simulations as part of these efforts. They are: (1) Input mesh and geometry information using FMDB [13], a flexible distributed mesh database developed in SCOREC. (2) Localization of the ordering of degree-of-freedom (DOFs), distributed vector and matrix objects and operations so as to allow M3D-C^l to perform all operations needed by the matrix solvers locally, thus hiding the complexity of parallel operations. (3) Access to the distributed matrix storage data structure to assemble matrices for PETSc solvers to effectively apply the PETSc scalability and preconditioning technologies developed by TOPS. (4) Anisotropic size-driven mesh adaptation including solution field transfer during local mesh modifications.

6. Adaptive Meshing

The M3D-C^l simulations often exhibit high gradients in localized areas of the domain. Using uniform meshes with small mesh size over the entire domain will over-refine the regions beyond the critical local domains with high gradients which can lead to infeasible simulations. Size-driven mesh adaptation [14] based on error indicators is an effective means to resolve this issue by structuring the mesh domains with elements concentrated in the domains needed to improve computational efficiency and accuracy. ITAPS and SCOREC have successfully introduced the size-driven mesh adaptation procedure in M3D-C^l to account for anisotropic solution characteristics. Interpolation-based error indicators [15] have been employed to compute the mesh size field needed by the mesh adaptation. Anisotropic adaptivity is quite effective in further reducing the number of elements needed for a given level of solution accuracy where the solution gradients are stronger in specific directions as is commonly the case in contained plasma fields.

7. Results of a linear stability application

As part of our verification process, we are computing linear unstable eigenmodes of a fairly simple toroidal configuration that can be evaluated by other codes in the appropriate limits. Using the parameterization described in [7], we defined a near circular cross section toroidal plasma of minor radius 1.0 and major radius 3.0, centered inside a conducting vacuum vessel of dimension 3x3. Defining an equilibrium toroidal field $RB_T = 2.25$, we calculated an equilibrium with plasma current $\mu_0 I_p = 0.7$, central safety factor $q_0 = 1$, central pressure and derivative $p_0 = 0.030$, $p_1 = -0.5$. The resistivity varied as $p^{-3/2}$, going from 2.5×10^{-6} in the center to 0.415 at the edge and in the region outside the plasma. We show the perturbed values of ψ in Figure 1. These had corresponding growth rates 0.078, 0.1060, and 0.1180, obtained by solving the time-dependent equations for 100 cycles with a time step $\delta t = 2.0$. The mesh used is shown in Figure 1d, superimposed upon colors showing the resistivity contours. It is seen to be fine in the plasma region, continuously varying to coarse in the 'vacuum' region. The growth rates obtained were the same to 3 digits when a uniform mesh was used with the same fineness as used here only in the plasma region, but this required 14,400 vertices as opposed to the 6,245 vertices used here.

8. Summary

The M3D- C^l code has been extended to 3D in toroidal geometry. This paper describes a subset of the full code that is single fluid MHD linearized about an equilibrium without flow. Future publications will build on the structure and algorithm described here to extend it to a full nonlinear 3D solution of the 2F MHD equations. The implicit time advance splits into two parts: the velocity advance described by (6abc), and the field advance described by (7ab). The magnetic field is manifestly divergence free. Energy conserving subsets of the full equations (reduced MHD) are obtained by solving only (6a) and (7a), or only (6ab) and (7ab). The SCOREC adaptivity software is shown to greatly increase the efficiency of the calculation.

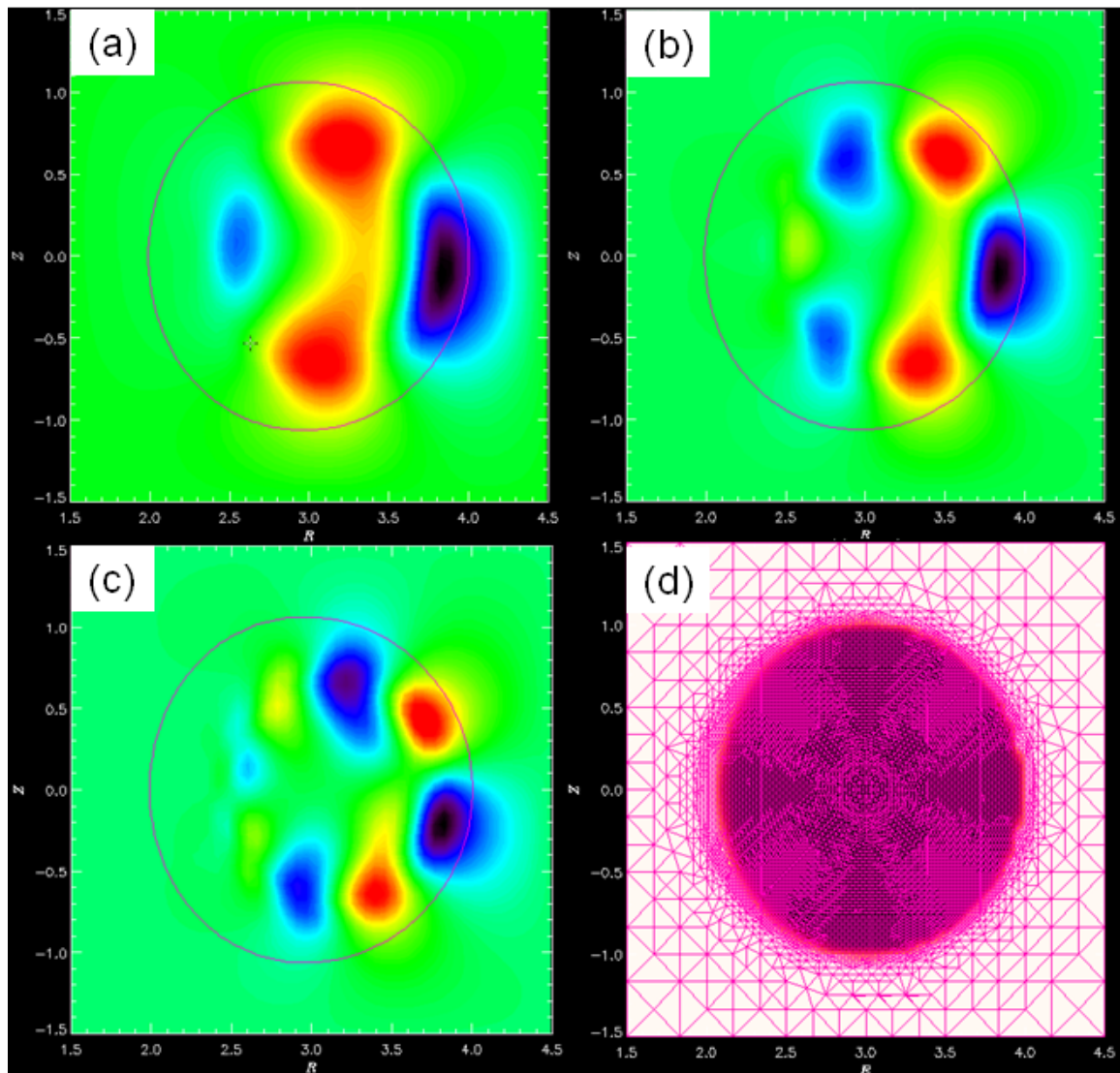


Figure 1: The M3D- C^l code is being benchmarked by computing unstable modes in a circular cross section toroidal plasma. Shown are eigenmodes of ψ for modes with toroidal mode # (a) $n=1$, (b) $n=2$, and (c) $n=3$. In (d) is the unstructured mesh superimposed on the equilibrium resistivity contours.

Acknowledgment

This work was supported by U.S. DoE contracts DE-FC02-06ER25760 and DE-AC02-76CH03073. The authors benefitted from discussions with Drs. M. Chance, G. Fu, W. Park, H. Strauss, and L. Sugiyama, and from discussions and assistance from Drs. A. Bauer and Y.S. Li.

Appendix

The partial energy terms, $\delta W_{kj}(a_k, b_j)$ are obtained by taking the integral of the inner product of the k^{th} velocity component with the operator L operating on the j^{th} velocity component. For example: $\delta W_{13}(U, \chi) \equiv R^2 \nabla U \times \nabla \varphi \cdot L \{ R^2 \nabla_{\perp} \chi \}$. In implementing the Galerkin method, each finite element basis function is used in place of the first variable and the second variable is expanded in basis functions. Integration by parts are done so that no more than two derivatives appear on any scalar, consistent with restrictions on C^1 elements. The 9 integrands are as follows:

$$\begin{aligned} \delta W_{11}(v_i, U) = & -\frac{1}{R^2} (R^2 [U, \psi], R^2 [v_i, \psi]) + \Delta^* \psi [v_i, R^2 [U, \psi]] - \frac{F}{R^2} (U', R^2 [v_i, \psi]) \\ & + \frac{F}{R^2} (R^2 [U', \psi], v_i) + \Delta^* \psi F [v_i, U'] + \frac{F^2}{R^2} (U'', v_i) + R^2 [v_i, R^2 [U, p]] + 2R^2 \gamma [v_i, p U_z] \end{aligned}$$

$$\delta W_{12}(v_i, \omega) = \omega' \frac{1}{R^2} (\psi, R^2 [v_i, \psi]) - \omega' \Delta^* \psi [v_i, \psi] - \frac{F}{R^2} (\omega'' (\psi, v_i)) - R^2 \gamma [v_i, p \omega']$$

$$\begin{aligned} \delta W_{13}(v_i, \chi) = & \frac{1}{R^2} (R^2 (\chi, \psi), R^2 [v_i, \psi]) - \Delta^* \psi [v_i, R^2 (\chi, \psi)] + \frac{F}{R^4} [R^2 [v_i, \psi], \chi'] \\ & - \frac{F}{R^4} ((\chi', \psi), v_i) + \Delta^* \psi \frac{F}{R^4} (\chi', v_i) + \frac{F^2}{R^4} [\chi'', v_i] + 2v_i \frac{1}{R^2} [(\chi, p) + \gamma p \Delta^* \chi] \end{aligned}$$

$$\delta W_{21}(v_i, U) = R^2 [\psi, F] [U, v_i] - \frac{v_i}{R^2} (R^2 [U', \psi], \psi) - v_i \frac{F}{R^2} (U'', \psi) + v_i F [F, U'] - v_i R^2 [U', p] - 2v_i \gamma p U'_z$$

$$\delta W_{22}(v_i, \omega) = -R^2 [v_i, \psi] [\omega, \psi] + v_i \frac{\omega''}{R^2} (\psi, \psi) - v_i \omega' [F, \psi] + \gamma v_i p \omega''$$

$$\begin{aligned} \delta W_{23}(v_i, \chi) = & + \frac{v_i}{R^2} (R^2 (\chi', \psi), \psi) - \frac{F}{R^4} (R^2 [v_i, \psi], \chi) + R^2 (\chi, \psi) [F, v_i] \\ & - \frac{v_i}{R^4} (F [\chi'', \psi]) + v_i \frac{F}{R^4} (F, \chi') + (v_i R^2 (\chi', p) + v_i \gamma p R^2 \Delta^* \chi') \end{aligned}$$

$$\begin{aligned} \delta W_{31}(v_i, U'') = & -\frac{1}{R^2} (R^2 [U, \psi], R^2 (v_i, \psi)) + \frac{1}{R^4} \Delta^* \psi (R^2 [U, \psi], v_i) - \frac{F}{R^4} [v_i, R^2 [U', \psi]] - \frac{F}{R^2} (U', R^2 (v_i, \psi)) \\ & + \Delta^* \psi \frac{F}{R^4} (U', v_i) - \frac{F^2}{R^4} [v_i, U''] + [F, U] F \left[\Delta^* v_i \frac{1}{R^2} + \left(\frac{1}{R^2}, v_i \right) \right] - \Delta^* v_i \left[[U, p] + \gamma \frac{2}{R^2} p U_z \right] \end{aligned}$$

$$\delta W_{32}(v_i, \omega) = + \frac{\omega'}{R^2} (\psi, R^2 (v_i, \psi)) - \Delta^* \psi \frac{\omega'}{R^4} (\psi, v_i) + F \frac{\omega''}{R^4} [v_i, \psi] - F [\omega, \psi] \left[R^2 \Delta^* v_i + (R^2, v_i) \right] + \Delta^* v_i \frac{1}{R^2} \gamma p \omega'$$

$$\begin{aligned} \delta W_{33}(v_i, \chi) = & + \frac{1}{R^2} (R^2 (\chi, \psi), R^2 (v_i, \psi)) - \frac{1}{R^4} \Delta^* \psi (R^2 (\chi, \psi), v_i) + \left[\Delta^* v_i \frac{1}{R^2} + (R^2, v_i) \right] F \nabla \cdot \frac{F}{R^4} \nabla_{\perp} \chi \\ & + \frac{F}{R^6} [v_i, (\chi', \psi)] - \frac{F}{R^4} [\chi', R^2 (v_i, \psi)] + \frac{1}{R^6} \Delta^* \psi F [\chi', v_i] - \frac{F^2}{R^8} (\chi'', v_i) + \Delta^* v_i R^4 ((\chi, p) + \gamma p \Delta^* \chi) \end{aligned}$$

References

- [1] W. Park, E. Belova, G. Y. Fu, et al., *Phys Plasmas* **6**, 1796 (1999)
- [2] S. C. Jardin, J. Breslau, N. Ferraro, *J. Comput. Phys.*, **226** (2007) 2146
- [3] N. Ferraro and S. Jardin, *Phys Plasmas* **13** (092101) 2006
- [4] C. Sovinec, A. H. Glasser, G.A. Gianakon, et al, , *J. Comput. Phys.* **195** (2004) 355
- [5] E. Caramana, *J. Comput. Phys.* **96** (1991) 484
- [6] I. Bernstein, E. Frieman, M. Kruskal, and R. Kulsrud, *Proc. Royal Soc.* 244 1740 (1958)
- [7] S. Jardin, *J. Comp. Phys.* **200** (2004) 133
- [8] H. Strauss, *Phys. Fluids* **19** (1976) 134
- [9] R. Hazeltine et al, *Phys Fluids* **28** (1985) 2466, R. Fitzpatrick et al, *Phys Plasmas* **11** (2004) 4713
- [10] R. Schmaltz, *Phys. Lett. A*, **82** 14 (1981)
- [11] R. Grimm, J. Greene, J. Johnson, in *Meth. Comput Phys.*, Academic Press, 1976
- [12] J. W. Demmell, J. R. Gilbert, Y. S. Li, *SUPERLU: Users Guide*, U. C. Berkeley, 2003
- [13] E. Seegyong, M.S Shephard, *Engineering with Computers* **22**:197—213 (2006)
- [14] X. Li, M.S. Shephard, M.W. Beall, *Comp. Meth. Appl. Mech. Engng.* **194**:4915--4950(2005)
- [15] O. Sahní , J. Muller, K.E. Jansen, M.S. Shephard. and C.A. Taylor , *Comput. Methods Appl. Mech. Engrg.* **195**(41-43):5634—5655 (2006)